

# Figure Captions

## Chapter 1

Figure 1-1 Energy diagrams of vacuum-metal boundary: (a) without external electric field; and (b) with an external electric field

Figure 1-2 The schematic diagram of (a) conventional cathode ray tube (CRT), (b) field emission display (FED)

Figure 1-3 The SEM micrograph of (a) Spindt type triodes array, (b) Spindt type field emission triode, and the schematic image of (c) Spindt type triode array

Figure 1-4 The FED products based on Spindt type field emitters, (a) motorola 5.6" color FED, (b) Pixtech 15" color FED, (c) Futaba 7" color FED and (d) Sony/Candescent 13.1" color FED

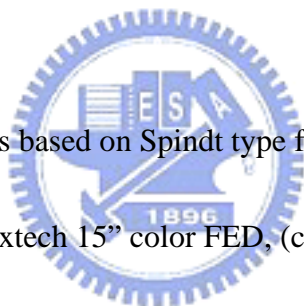


Fig. 1-5 (a) Si tip formed by isotropic etching and (b) Si tip field emission triodes array formed by CMP (c) cross section view of double gate Si field emitter arrays

Fig. 1-6 (a) SEM image of CNT cathode from Samsung's FED, (b) a 4.5-inch FED from Samsung, the emitting image of fully sealed SWNT-FED at color mode with red, green, and blue phosphor columns, and (c) a prototype of 5" CNT flat panel display by Samsung

Figure 1-7 (a) Fabrication of tunneling nano-gap (b) structure of SED (c) a 36-inch prototype of surface conduction electron emitter display

## Chapter 2

Figure 2-1 Experimental procedures for CNTs synthesized using SiO on Fe as the precursor. (a) Patterned Si substrate by lithography, (b) deposition of catalyst layer and inactive layer, (c) photoresist lift-off and (d) carbon nanotube growth.

Figure2-2 Schematic diagram of high-vacuum field-emission measurement apparatus

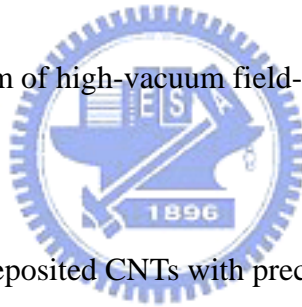


Figure2-3 SEM images of deposited CNTs with precursor of 3.5nm Fe.(a) 60° top view and (b) cross sectional view.

Figure2-4 Schematic illustration of electron field-emission vs applied electric field. (a) The static electric field of CNTs, (b) electrons emitted from edge region of CNT film as applied field exceeded turn-on electric field and (c) electrons emitted from center part of CNTs at higher applied field.

Figure2-5 SEM images of deposited CNTs with precursor of 3.5nm/3.5 nm SiO/Fe. (a) 60° top view and (b) the cross-sectional view.

Figure2-6 SEM images of deposited CNTs with precursor of 7.5 nm/3.5 nm SiO/Fe.

(a) Low magnification view, and (b) and (c) 60° tilted views.

Figure2-7 SEM images of deposited CNTs with precursor of 15 nm/3.5 nm SiO/Fe. (a) Low magnified view, and (b) and (c) 60° tilted views.

Figure2-8 Growth mechanism of CNTs with SiO and Fe as the precursor. (a) SiO 3.5nm/Fe 3.5nm, (b) SiO 7.5nm/Fe 3.5nm and (c) SiO 15nm/Fe 3.5nm

Figure2-9 Field emission properties of CNTs deposited with SiO/Fe films as precursors. (a) Field-emission current density vs applied field. (b) Corresponding F-N plot.

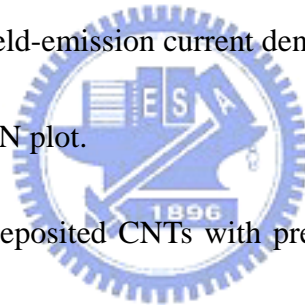


Figure2-10 SEM images of deposited CNTs with precursor of 5.0nm Fe. (a) 60° top view and (b) cross sectional view.

Figure2-11 (a) and (b) Low magnification view of SEM images of deposited CNTs with precursor of 1.5nm/5.0 nm SiO/Fe.

Figure2-12 (a) and (b) Low magnification view of SEM images of deposited CNTs with precursor of 7.0 nm/3.5 nm SiO/Fe.

Figure2-13 (a) and (b) Low magnification view of SEM images of deposited CNTs with precursor of 15 nm/3.5 nm SiO/Fe.

Figure2-14 Field emission properties of CNTs deposited with SiO/Fe films as

precursors. (a) Field-emission current density vs applied field. (b)

Corresponding F-N plot.

## Chapter 3

Figure 3-1 SEM images of CNTs grown using partial oxidation of metal catalyst

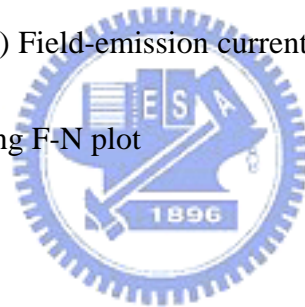
(a) low magnification of top view (b) low magnification of 60°top view

(c) high magnification of 60°top view (d) the cross-sectional view.

Figure 3-2 Field emission characteristics of CNTs grown using partial oxidation of

metal catalyst (a) Field-emission current density vs applied electric field.

(b) Corresponding F-N plot



## Chapter 4

Figure 4-1 AFM images of iron film under different pre-treatment time

( a ) only annealing ( b ) 5 min pre-treatment

( c ) 10 min pre-treatment

Figure 4-2 SEM images of iron film under different pre-treatment time

( a ) only annealing ( b ) 5 min pre-treatment

( c ) 10 min pre-treatment

Figure 4-3 SEM images of CNTs grown under different pre-treatment time

( a ) 5 min pre-treatment

( b ) 10 min pre-treatment

Figure 4-4 Field emission properties of CNTs grown under different pre-treatment

times. (a) Field-emission current density vs applied electric field. (b)

Corresponding F-N plot.

Figure 4-5 SEM images of CNTs grown under 10% hydrogen content during  
pre-treatment( H<sub>2</sub>/N<sub>2</sub>: 100sccm/900sccm). (a) 60° top view and (b)  
the cross-sectional view.



Figure 4-6 SEM images of CNTs grown under 30% hydrogen content during  
pre-treatment( H<sub>2</sub>/N<sub>2</sub>: 300sccm/700sccm). (a) 60° top view and (b)  
the cross-sectional view.

Figure 4-7 SEM images of CNTs grown under 50% hydrogen content during  
pre-treatment( H<sub>2</sub>/N<sub>2</sub>: 500sccm/500sccm). (a) 60° top view and (b)  
the cross-sectional view.

Figure4-8 Field emission properties of CNTs grown under different hydrogen

content (a) Field-emission current density vs applied electric field. (b)

Corresponding F-N plot

## Chapter 5

Figure5-1 SEM images of pillars of CNTs with R/H ratio of 1/3. (a) and (b) show low magnification view, and (c) and (d) cross-sectional views of different magnification.

Figure5-2 SEM images of pillars of CNTs with R/H ratio of 2. (a) and (b) show low magnification views. (c) cross-sectional view

Figure5-3 Field emission characteristics of pillars of CNTs with R/H ratio of 2.3. (a) Field-emission current density vs applied field. (b) Corresponding F-N plot.

Figure5-4 Field emission properties of pillars of CNTs with R/H ratio of 1/3. (a) Field-emission current density vs applied field. (b) Corresponding F-N plot.

## Chapter 6

Figure 6-1 Fabrication procedures for CNTs treated by O<sub>2</sub> plasma etching.

Figure 6-2 SEM images of CNTs treated with 60 s O<sub>2</sub> PPT for different ICP powers

of (a) non-PPT, (b) 250 W, (c) 400 W and (d) 600 W.

Figure 6-3 SEM images of CNTs treated by PPT for different ICP plasma etching times (a) 30 s, (b) 60 s and (c) 90 s. The ICP plasma power was held at 400 W.

Figure6-4 Raman spectra of CNTs under various lengths of O<sub>2</sub> plasma post-treatment.

Figure 6-5 Raman spectra of CNTs under O<sub>2</sub> plasma post-treatment at various powers.

Figure 6-6 TEM images of CNTs (a) before and (b) after O<sub>2</sub> plasma post- treatment. The plasma power and treatment time were 400 W and 60 s, respectively.



Figure 6-7 (a) Characteristics of emission current density (J) vs applied electric field (E) for CNTs with different RF plasma power treatments. The plasma etching time is 60 s. (b) corresponding FN plots.

Figure 6-8 Characteristics of emission current density (J) vs applied electric field (E) for CNTs with different etching times, but constant RF power at 400 W.

Figure 6-9 Characteristics of emission current density (J) vs applied electric field

(E) for CNTs with different etching times, but constant RF power at 250 W.

Figure 6-10 Emission current stability of CNTs after plasma treatment over period of 1500 s. The RF power was kept at 400 W and the plasma etching time was 60 s.

## Chapter 7

Figure 7-1 Schematic representation of fabrication procedures for vertical CNT LFED.

Figure7- 2 (a) SEM micrograph of vertical CNT LFED for SiO<sub>2</sub> lateral etching time of 16 min. (b) Cross-sectional SEM micrograph of CNT diode showing anode-to-emitter gap of 1.84 μm.

Figure7- 3 (a) SEM micrograph of vertical CNT LFED for SiO<sub>2</sub> lateral etching time of 7 min. (b) Cross-sectional SEM micrograph of CNT diode showing anode-to-emitter gap of 0.53 μm.

Figure 7-4 (a) Emission current ( $I_a$ ) and anode voltage ( $V_a$ ) characteristics of vertical CNT LFED for different anode-to-emitter gaps, and (b) corresponding F-N plots.



Figure 7-5 Cross-sectional SEM micrographs of vertical CNT LFED showing different CNT lengths: (a)  $0.26 \mu\text{m}$ , (b)  $0.6 \mu\text{m}$ , and (c)  $2.46 \mu\text{m}$ .

Figure 7-6 (a) Emission current ( $I_a$ ) and anode voltage ( $V_a$ ) characteristics of vertical CNT LFED with different heights of CNTs, and (b) corresponding F-N plots.

Figure 7-7 Emission current reliability of vertical CNT LFED.

The anode-to-emitter gap is  $0.55 \mu\text{m}$ . (a) CNT growth time of 8 min. (b) CNT growth time of 20 min.

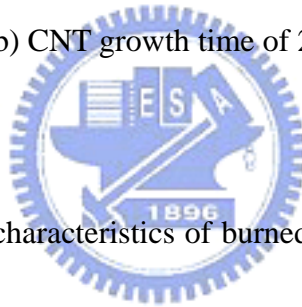


Figure 7-8 Field emission characteristics of burned-out carbon nanotubes under strong electrical field

Figure 7-9 (a) SEM micrograph of vertical CNT LFED for original CNT morphology. (b) SEM micrograph of the CNTs LFED with burned-out or flew away CNTs.

Figure 7-10 Emission current stability of the vertical CNT LFED over a period of 1500s.